EARTH SURFACE PROCESSES AND LANDFORMS Earth Surf. Process. Landforms **36**, 1268–1278 (2011) Copyright © 2011 John Wiley & Sons, Ltd. Published online 8 April 2011 in Wiley Online Library (wileyonlinelibrary.com) DOI: 10.1002/esp.2155

Real-time measurement and preliminary analysis of debris-flow impact force at Jiangjia Ravine, China

Kaiheng Hu,1,2* Fangqiang Wei1,2 and Yong Li1,2

- ¹ Key Laboratory of Mountain Hazards and Earth Surface Processes, Chinese Academy of Sciences, Chengdu, China
- ² Institute of Mountain Hazards and Environment, Chinese Academy of Sciences, Chengdu, China

Received 17 March 2010; Revised 9 February 2011; Accepted 14 February 2011

*Correspondence to: Kaiheng Hu, Key Laboratory of Mountain Hazards and Earth Surface Processes, Chinese Academy of Sciences, Chengdu 610041, China. E-mail: khhu@imde.ac.cn



Farth Surface Processes and Landforms

ABSTRACT: Impact forces associated with major debris flows (Jiangjia Ravine, China, August 25, 2004) were recorded in real time by a system consisting of three strain sensors installed at different flow depths. This provides the first real-time and long-duration record of impact forces associated with debris flows. A comprehensive approach including low-pass filtering and moving average methods were used to preprocess the recorded signals. The upper limit of impact frequency in the debris flows was estimated at 188-66 Hz under the assumption that only coarse grains cause effective impact loadings. Thus, a low-pass filter with a 200 Hz cut-off frequency was needed to denoise the original data in order to extract the impact force. Then the moving average method was applied to separate long-term and random components of the filtered data. These were interpreted as, respectively, the fluid pressure and grain impact loading. It was found that the peak grain impacts at different depths were non-synchronous within the debris flows. The impact loadings were far greater than, and not proportional to the fluid pressures. Analysis of the impact force of 38 debris flow surges gives an empirical value for the ratio of the hydrodynamic pressure to the momentum flow density, i.e. the product of debris-flow density and mean velocity square, which provides a very valuable basis for understanding debris flow dynamics and designing debris flow management systems. Copyright © 2011 John Wiley & Sons, Ltd.

KEYWORDS: debris flow; impact force; hydrodynamic pressure; Jiangjia ravine

Introduction

Debris flows cause damage mainly in three ways: deposition, erosion and direct impact. Impact often causes structural destruction and is the key element in engineering design and risk assessment (Mizuyama, 1979; Hungr *et al.*, 1984; Armanini and Scotton, 1993; Armanini, 1997; Zhang, 1993; Liu *et al.*, 1997; D'Agostino and Casonato, 2000; Haehnel and Daly, 2004; Zanuttigh and Lamberti, 2006; Wendeler *et al.*, 2007; Zhang *et al.*, 2007; Shieh *et al.*, 2008; Hübl *et al.*, 2009). However, the impact mechanism so far is poorly understood, partly due to the difficulties in measuring impact forces.

The acquisition and analysis of debris-flow impact forces under real-world conditions have been a challenge for scientists and engineers for a long time. Until now, a few field experiments have been carried out, such as at Mt Yakedake in Japan (Suwa *et al.*, 1973; Okuda *et al.*, 1977); Jiangjia Ravine in China (Zhang and Yuan, 1985; Zhang, 1993; Hu *et al.*, 2006); and Illgraben torrent in Switzerland (Wendeler *et al.*, 2007). In addition, back-analyses of field investigations of structural failures have yielded a rough estimation of impact forces (Hungr *et al.*, 1984; Revellino *et al.*, 2004; Zanchetta *et al.*, 2004). Hungr *et al.* (1984) provided an empirical formula to estimate the thrust force of debris flow and point impact load

of boulders in the flow directed against structural barriers, based on two years of study in the coastal and interior regions of British Columbia, Canada. On the basis of 70 impact-force records obtained from Jiangjia Ravine, Zhang (1993) summarized three kinds of impulsive forms: rectangular, saw-toothed, and peak impulse. However, there has been little substantial progress on real-world debris-flow impact forces. Recently, many small-scale flume experiments have been performed in order to develop theoretical models for the calculation of impact force, with the goal of engineering optimization and risk evaluation (Armanini and Scotton, 1993; Wei, 1996; Lin et al., 1997; Liu et al., 1997; Scotton and Deganutti, 1997; Haehnel and Daly, 2004; Wei et al., 2006; Zhang et al., 2007; Shieh et al., 2008). However, Hübl et al. (2009) found that Froude numbers of field and laboratory data fall in different ranges, suggesting that the models developed from laboratory data may not replicate or be comparable with field data.

The destructive power of debris flow consists of surface pressure due to fluid-phase slurry thrusting, and point-wise loading due to coarse solid particle collision. The fluid pressure, including hydrostatic and hydrodynamic components, strongly depends on fluid density, flow depth, velocity, and impact angle, while the solid loading depends on the velocity and size of the largest boulder, as well as the geometry

and properties of the structures subject to collision. Armanini and Scotton (1993) observed that the internal global viscosity of a debris-flow mixture influences impact behavior. Low viscosity flow will be completely deviated so as to form a vertical jet-like bulge when impacting a barrier, and high viscosity flow will form a reflecting wave that propagates upstream. Corresponding to the two parts of the impact force, the computational models can be categorized into hydraulic and solid collision models (Hübl et al., 2009). The solid models are usually based on the Hertz equation which relates the impact loading to contact deformation or to structural deflection of elastic or elastic-plastic materials (Mizuyama, 1979; Hungr et al., 1984; Zhang, 1993). The hydraulic models are mainly derived from fluid momentum balance and the Bernoulli equation, and are further classified into hydrostatic, hydrodynamic, mixed, shock wave, and full models (Table I). The impact load due to cobbles and boulders is more complex and more unpredictable than the fluid pressure. Therefore, hydraulic models have been proved more popular and practicable than solid collision models. Of course, sometimes hydraulic models may underestimate the impact force, especially when there are large boulders in the flow. From our point of view, the better choice is to develop a solid-fluid-coupled model. But, at present there are insufficient field data, and a reliable approach to obtain both the fluid pressures and impact loads has yet to be achieved.

This paper reports an *in situ* test of debris-flow impact at Jiangjia Ravine on August 21–25, 2004, and introduces a simple approach to separate the two components of the impact force. Impact forces were measured by three strain sensors at different flow depths, and high-frequency noise in the original data were filtered by applying an upper limit frequency estimated from the grain size distribution. A moving-average approach was applied to separate the fluid pressure from the grain-impact loading. Finally, a preliminary analysis was made of the relationships of mean velocity versus hydrodynamic pressure, and hydrodynamic pressure versus grain-impact loading with the measured data.

Background of Measurement

Study area

Jiangjia Ravine, a tributary of Xiaojiang River in the upper reaches of the Yangtze River, is located near the city of Dongchuan, Yunnan Province, in south-western China (Figure 1). The ravine has 2227 m of relief, 48.6 km^2 of area and 13.9 km of mainstream length. The annual rainfall is between 700 mm to 1200 mm. Debris flows occur in the rainy season (from June to September) in which more than 80% of the annual rainfall occurs. Jiangjia is well-known for its high frequency of debris flows, up to 28 times in 1965. With the predictable occurrence, the basin has been an ideal site for observation and research on debris-flow formation, movement and deposition. Long-term observations show that the flow bulk density ranges from 1600 to 2300 kg m⁻³ and that the volumetric solid fraction ranges up to 85% (Li and Yuan, 1983; Zhang, 1993; Cui et al., 2005). The initial attempts to measure the impact processes of debris flows in situ took place between 1973 and 1975 (Zhang and Yuan, 1985). The impulsive processes of 59 debris-flow surges had been recorded since the late 1980 s, associated with improvements in measurement technique and instrumentation (Wu et al., 1990). Unfortunately, only a small part of the data was analyzed and published, and the instrumentation was destroyed by subsequent debris flows.

Observations and measurements

On August 21, 2004, a new system of instrumentation was set up at the middle reach of the Jiangjia drainage to acquire data on the impulsive processes of debris flow (Figure 1). The system is composed of a steel pile foundation with strain sensors and auxiliary instruments, such as an ultrasonic sensor, to record the flow depth, and a sampler to collect the debrisflow sample (Figure 2). The selected reach was 130 m long and 22 m wide, shown along the dashed lines in Figure 1a. Two control sections at the ends of the reach were chosen in order

Table I. Summary of hydraulic models

Author	Formula	Coefficient or parameters	Data source	Description		
Hungr <i>et al.</i> (1984)	$p = c_d \rho v^2 \sin \varphi$	$c_d = 1.5$	Back-analysis data in British Columbia, Canada	Hydrodynamic model		
Armanini and Scotton (1993)	$p = c_s \rho g H$	$c_s = 4.5$	Laboratory experiments	Hydrostatic model incorporating dynamic pressure into static pressure		
Zhang (1993)	$\rho = c_d \rho v^2 \mathbf{cos}^2 \alpha$	$c_d = 3 \sim 5$	Field measured data in Jiangjia Ravine, China	Hydrodynamic model		
Wei (1996)	$p = 0.5\rho gH + \rho_c v_c v$		Laboratory experiments	Shock wave model		
Scotton and Deganutti (1997)	$p = c_s \rho g H$	$c_s = 2.5 \sim 7.5$	Laboratory experiments	Hydrostatic model		
Liu <i>et al.</i> (1997)	$p = \rho g \cos \theta h + \rho g \sin \theta L_0$ $-\frac{\tau_0 L_0}{h} + \frac{\rho}{2} v^2 _{-L_0} + \rho v_f v _{-L_0}$		Laboratory experiments	Full model including static pressure, weight of the debris volume, bottom stress, dynamic pressure and shock effect		
Arattano and Franzi (2003)	$\rho = c_m(0.5\rho gH + \rho v^2)$	$c_m = 1.0$	Field measured data in Moscardo torrent, Italy	Mixed model including hydrostatic and hydrodynamic pressures		
Hübl and Holzinger (2003)	$\rho = 5\rho (gH)^{0.6} v^{0.8}$		Field and laboratory experimental data	Modified hydrodynamic model		

Note: p is the impact pressure (in N m⁻²), c_d , c_s and c_m are the dimentionless coefficients of hydrodynamic, hydrostatic and mixed models, ρ the debris-flow density (in kg m⁻³), v the debris-flow velocity (in m s⁻¹), φ the least angle between the face of the barrier and the flow direction, g the gravity acceleration (in m s⁻²), H the flow depth (in meters), α the angle between the flow direction and the direction normal to the impacting plane, ρ_c the maximum density of impacted debris flow (in kg.m⁻³), v_c the pressure shock wave velocity (in m s⁻¹), θ the slope angle, τ_0 the yield stress (in N m⁻²), h the flow depth at a distance L_0 from an obstacle (in meters), and v_f the phase speed of the flow front (in m s⁻¹).

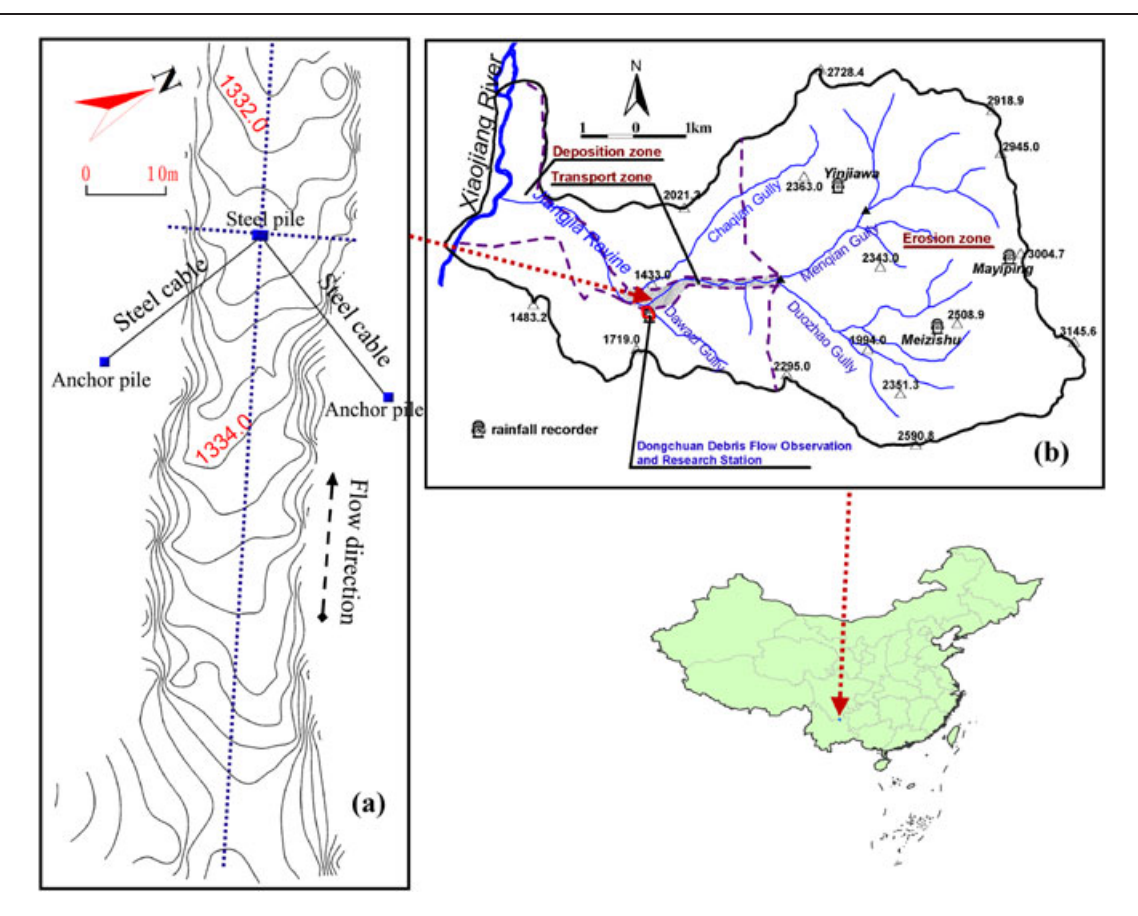


Figure 1. Maps of the observed channel (a) and Jiangjia Ravine (b) (Dongchuan Debris Flow Observation and Research Station located on the side of the transport reach was founded by the Chinese Academy of Sciences in 1961. Three rainfall gauges at Yinjiawa, Mayiping and Meizhishu can provide real-time rainfall per minute. The dotted lines in the left map correspond to longitudinal and transverse sections shown in Figure 3.). This figure is available in colour online at wileyonlinelibrary.com/journal/espl

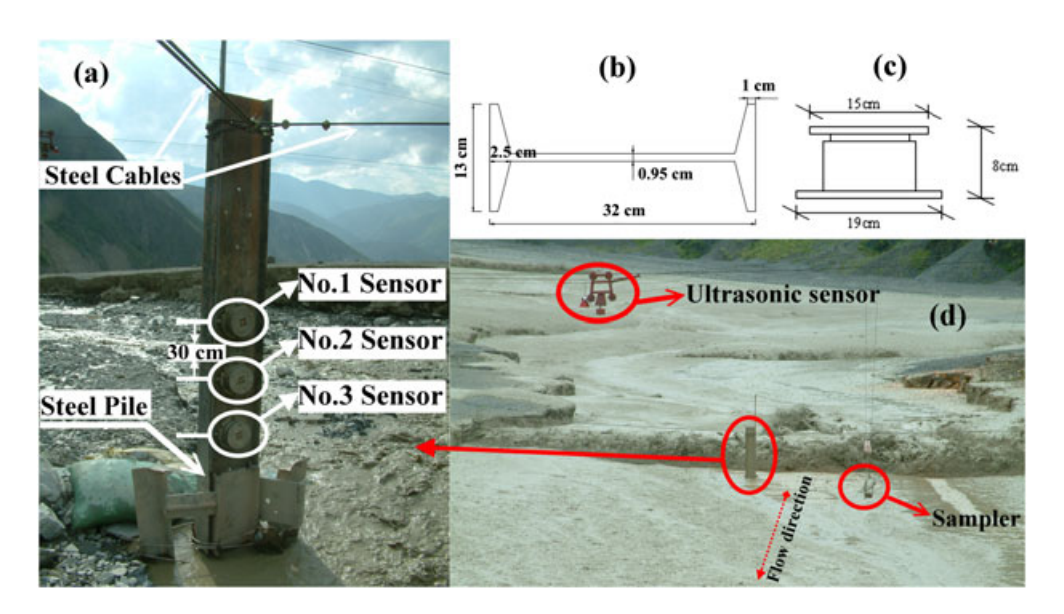


Figure 2. Measurement set-ups: (a) front view of steel pile before the event, (b) cross-section of the steel pile, (c) side view of the sensors, and (d) Bird's eye view of experimental field from downstream. The ultrasonic sensor was about 6·0 m high over the channel bed, and the length of the pile above the bed was 1·8 m in (d). This figure is available in colour online at wileyonlinelibrary.com/journal/espl

to measure mean velocity of the fronts of debris-flow surges. The longitudinal and transverse profiles across the steel pile are shown in Figure 3. Mean slope of the reach was 5.22%. The top of the steel column, about 2.5 m over the bed, was fixed by two sets of steel cables of 1.2 cm diameter, secured to concrete anchor piles on both sides of the channel. The strain sensors are vertically arrayed on the pile front with a uniform interval

of 30 cm, and the lowest sensor is 65 cm above the bottom. The impact sensors were designed and made by the Facility Design and Instrumentation Institute, China Aerodynamics Research and Development Center, and calibrated by the Chengdu Institute of Metrology Supervision and Verification with the standard dynamometer which satisfies Chinese National Metrological Verification Regulation. The sensors

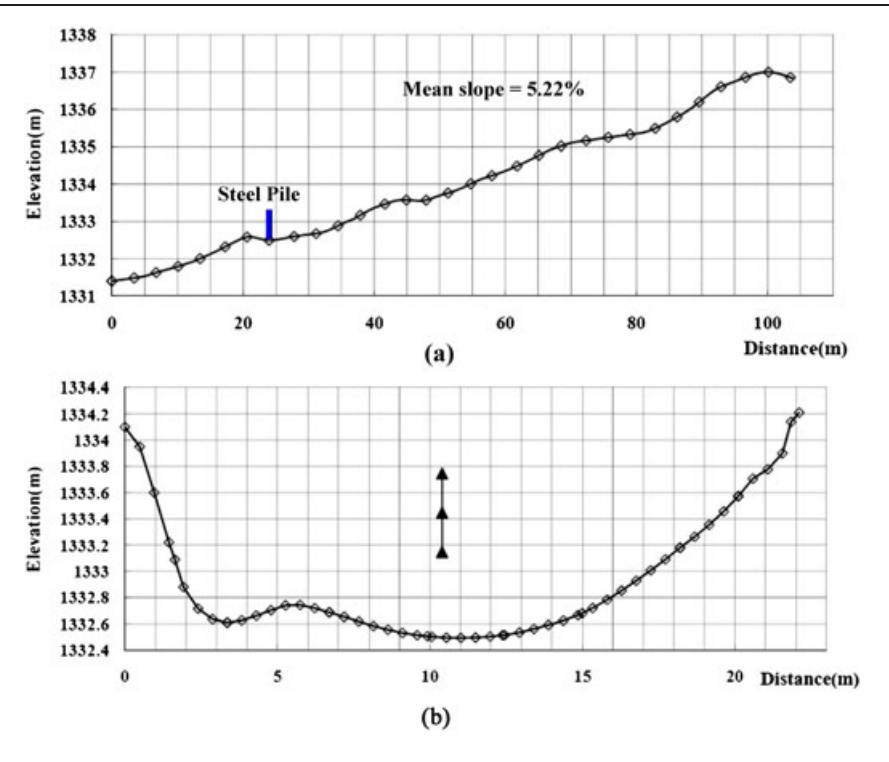


Figure 3. Longitudinal (a) and transverse (b) profiles of the observed channel along the dotted lines. (The triangle symbols in (b) denote the impact sensors. The vertical distance between the first and third sensors was 60 cm.). This figure is available in colour online at wileyonlinelibrary.com/journal/espl

have a full scale range of 100 kN, and excellent accuracy as well as a high frequency response (Table II). The sampler is a 61 cm high cylinder container with 18 cm inner diameter. Initially, the sampler was placed close to the bed, and then raised by hanging cables and a pulley after the flows passed. Theoretically, it is possible to collect coarse grains as large as 18 cm. But in practice, grains above 10 cm in collected samples were rare. The sample bulk density is estimated by the ratio of its mass to its volume.

Debris flows on August 25, 2004

On August 25, 2004, short intense rainfall from 11:24 a.m. to 13:14 p.m. triggered a moderate-scale debris-flow event. The accumulative rainfall was 17·6 mm, and maximum intensity was 1·4 mm per minute according to data from the Mayiping rain gauge. Debris flows arrived at the observed section at 12:40, and terminated at 15:00. Forty-nine surges were identified by eye witnesses and a video camera, but only 38

were measured by the sensors. The mean velocity of the wave fronts was measured by the travel time between the two control sections, reaching a peak of $11\cdot79~\text{m s}^{-1}$ at 13:46.48. The peak discharge of $840\cdot0~\text{m}^3~\text{s}^{-1}$ occurred at 13:37.24. Maximum volume concentration was $68\cdot6\%$ at 13:22.30, equivalent to a bulk density of $2200~\text{kg m}^{-3}$, given that the rock density is $2750~\text{kg m}^{-3}$ in the study area. The volume concentration was reduced to $57\cdot1\%$ ($2000~\text{kg m}^{-3}$) one hour later, and to 44% ($1770~\text{kg m}^{-3}$) another 22~minutes later. The flows finally transformed into the sediment-laden stream.

Five samples were collected successfully from surge fronts or subsequent hyper-concentration flow, with three listed in Table III, having bulk densities of greater than 2000 kg m⁻³ and containing 20–30% by weight percentage of grains > 20 mm (Figure 4). The grain content of > 20 mm in the 21st surge is less than in the 10th and 30th surges. But that surge has more particles between 5 mm and 20 mm than the other two surges (Figure 4). Table III shows that the flow with the higher density can move faster, which implies that more particles between 5 mm and 20 mm could increase the velocity of the

Table II. Specification of the impact force sensors

Range	Supply voltage (V)	,		Maximum frequency (KHz)	Sensitivity (mV)	Resolution (N)	Accuracy (‰)
0–100	12	< 1	-20-70	8	0.1526	0.3052	<3

Table III. Properties of three debris-flow samples

Surge number	Sampling time	$ ho$ (kg m $^{-3}$)	<i>U</i> (m s ⁻¹)	V ₂₀₋₄₀ (%)	V ₄₀₋₈₀ (%)	V ₈₀₋₁₀₀ (%)	f (Hz)
10	13:22.00	2104	5.24	10.55	8.45	0.0	155·46
21	13:41.30	2180	6.59	8.28	5.48	0.0	179.95
30	14:01.45	2040	5.99	12.84	5.50	0.0	188-66

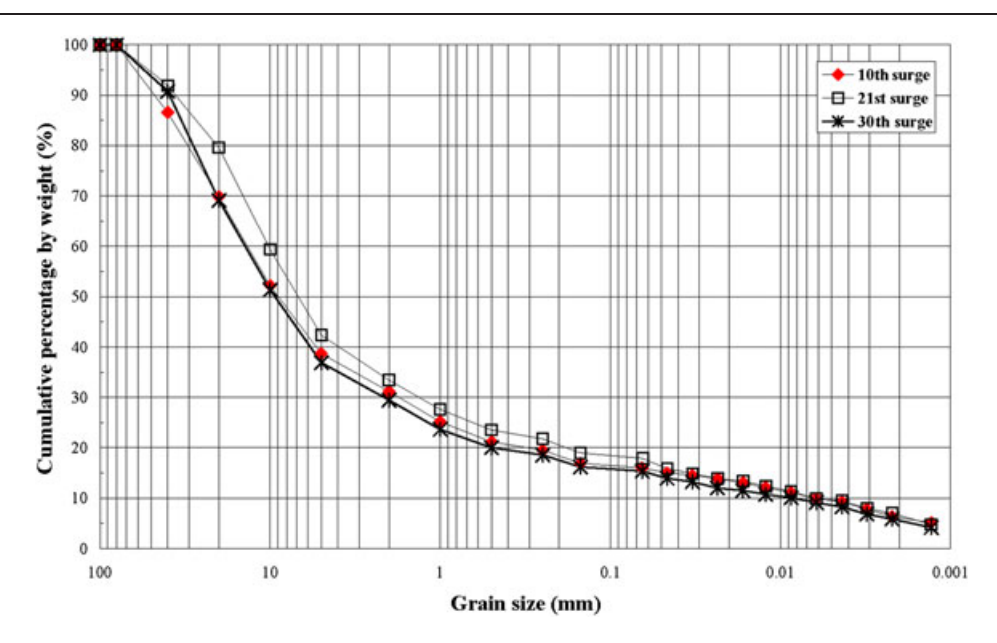


Figure 4. Cumulative grain size distribution of the three surges (the vertical axis is the percentage of weight of all grains smaller than one size to the total weight of a sample. The grain volume concentrations in Table III are derived from their weight percentage.). This figure is available in colour online at wileyonlinelibrary.com/journal/espl

Table IV. Maximum fluid pressure and grain impact loading of 38 surges measured by the three sensors

Surge number·	Arriving time	Flow depth (m)	Mean	Density $(10^3 \text{ kg} \text{ m}^{-3})$	Fluid pressure (kN m ⁻²)			Grain impact loading (kN m ⁻²)		
			velocity $(m s^{-1})$		Sensor 1	Sensor 2	Sensor 3	Sensor 1	Sensor 2	Sensor 3
3	13:09.33	1.50	6.74	2.10	33.95	28.42	10.13	39.87	38.85	78·11
4	13:11.09	1.50	7.44	2.10	53.81	92.40	110.76	137.41	116.05	312.94
5	13:12.19	1.50	6.25	2.10	82.64	63.78	25.71	172.50	189.23	497.09
6	13:14.26	1.50	6.02	2.10	36.53	21.80	25.60	75.89	21.74	31.35
7	13:15.05	1.60	6.34	2.10	60.79	52.30	63.91	78.16	107.99	88.40
8	13:16.36	1.20	6.87	2.10	52.79	34.35	35.11	1050.00	109.48	666.72
9	13:19.08	1.00	6.68	2.10	60.65	92.36	38.30	94.13	143.47	43.88
10	13:21.57	0.80	5.24	2.10	18.54	7.91	11.57	12.62	17.62	4.46
11	13:22.30	1.00	6.36	2.20	25.13	12.79	26.86	71·51	33.17	16.80
12	13:23.30	1.20	6.76	2.20	43.35	32.14	35.50	103.41	170.03	42.12
13	13:25.12	1.00	6.59	2.20	37.74	31.65	20.33	159.56	64.41	40.62
14	13:27.18	1.50	8.40	2.20	48.89	50.75	89.10	126.97	470.72	518.21
15	13:29.12	1.00	6.47	2.20	41.03	33.02	25.95	53.08	301.69	92.72
16	13:30.12	1.80	8.11	2.20	61.49	45.69	53.48	460.60	140.70	248.54
17	13:33.22	0.80	6.39	2.20	27.44	29.46	38.75	35.15	60.39	90.39
18	13:34.35	0.70	5.79	2.20	15.11	14.93	19.63	37.83	36.75	27.29
19	13:37.24	2.00	8.40	2.20	105.54	137.08	125.60	1109.90	1113.50	677.05
20	13:39.48	1.50	6.82	2.20	36.89	43.19	50.52	78.18	109.26	72.49
21	13:41.26	1.20	6.59	2.18	38.44	98.69	65.55	53.29	276.16	135.96
22	13:43.38	1.50	6.88	2.18	35.96	27.95	35.84	92.80	69.40	98.11
23	13:45.58	1.20	7.00	2.18	32.49	32.17	36.84	47.76	194.90	103.00
24	13:46.48	1.60	11.79	2.18	58.06	47.20	62.25	91.58	1089.50	223.76
25	13:51.07	1.60	7.72	2.18	58.89	45.24	54.09	268.94	679.88	1014.20
26	13:53.22	1.30	6.71	2.18	42.49	34.74	37.33	56.35	92.29	70.98
27	13:53.58	1.50	10.62	2.18	51.42	73.01	60.55	166.40	93.44	240.14
28	13:56.29	1.50	6.95	2.18	50.25	41.87	39.83	221.90	496.39	123.51
29	13:59.30	1.00	6.79	2.04	35.90	28.22	39.61	86.29	133.88	53.89
30	14:01.41	0.80	5.99	2.04	22.85	23.76	24.13	44.36	154.95	57.55
31	14:03.04	0.60	5.88	2.04	10.81	14.97	18.56	24.29	48.06	308.33
32	14:04.06	0.80	6.45	2.04	25.38	27.47	45.59	35.05	211.05	220.80
33	14:05.41	1.00	6.52	2.04	23.81	23.23	29.35	30.33	93.26	73.51
34	14:06.25	0.80	5.61	2.04	12.31	15.74	20.32	42.15	38.32	45.41
35	14:08.04	1.00	6.11	2.04	14.00	21.59	27.70	35.67	957.46	35.77
36	14:10.25	0.40	5.04	2.04	5.90	12.31	12.34	9.84	187.94	21.19
38	14:11.23	0.60	5.70	2.04	4.78	16.97	31.77	24.06	313.11	65.27
39	14:12.09	0.60	5.75	2.04	9.54	23.78	28.58	27.03	54.29	35.04
40	14:13.03	0.70	5.88	2.04	16.22	20.43	26.49	32.43	133.09	35.70
42	14:15.22	1.00	6.58	2.04	12.90	23.25	27.96	42.89	140.09	48.76

surge front. The bulk density of other surges was assigned to the density of one of the five samples according to their arrival time and behaviors (Table IV).

Large boulders > 30 cm were observed hitting the sensors (Figure 5). The sensors can bear a maximum load 20% greater than the full scale range, i.e. 120 kN. No recorded impulsive force exceeded the capacity. The measured signals show a typical shape for debris-flow surges, with a sharp front and a gently sloping tail, resembling pressures or flow-depth

hydrographs presented by other researchers (Iverson, 1997; Arattano, 2000; Marchi *et al.*, 2002). The channel bed was movable during the event, sometimes depositing and sometimes eroding. The change in bed elevation at the steel pile was up to 100 cm. The lowest sensor was buried by either sediment or slurry, so it measured much less impact than the other two (Figure 5). This observation agrees with that of Hungr *et al.* (1984) that inert debris material stopped by a barrier can shield the structure from subsequent impact.



Figure 5. Boulder stopped by the steel pile after debris flow passed by. (The third sensor was covered by slurry and debris deposits. It is easily noted that the bed elevation was changing and higher than that in Figure 2a.). This figure is available in colour online at wileyonlinelibrary.com/journal/espl

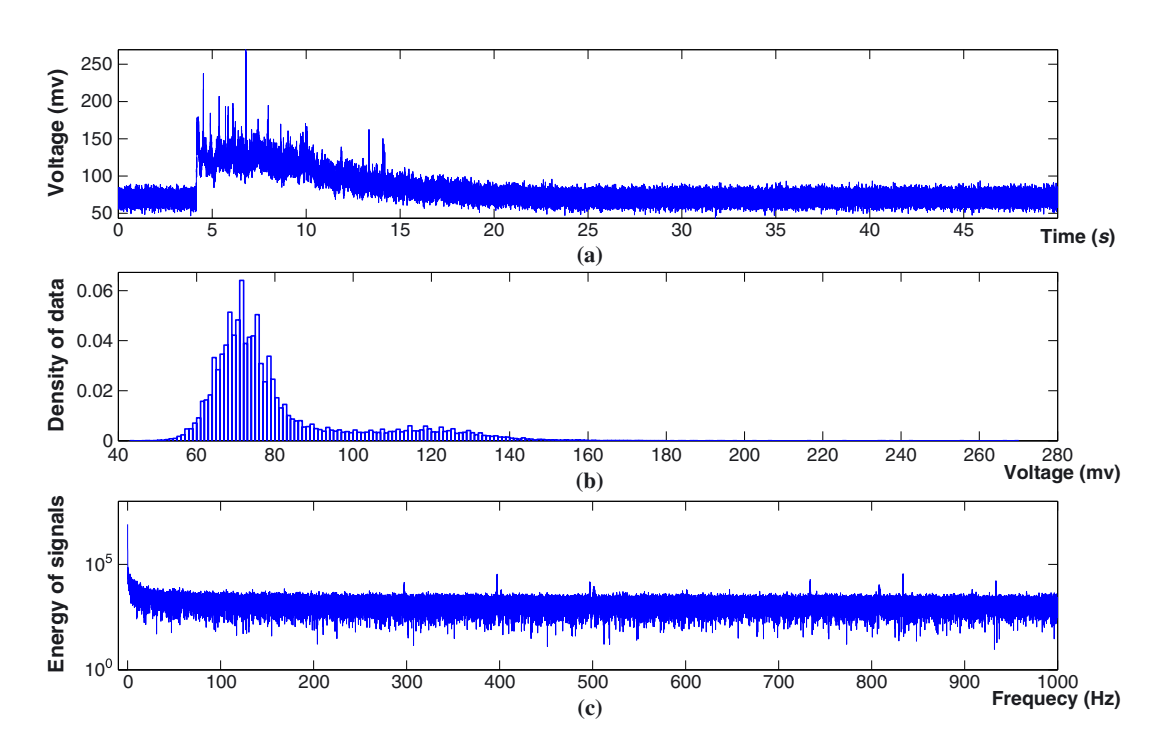


Figure 6. Original impulsive signal (a) of the 12th surge, its histogram (b) and energy spectrum (c). (The data shown here were collected by the first sensor, and the time origin of the signal is 13:23.30. The voltage value ranges from 43 to 269 mV, and the bin width of the histogram is 1 mV. The energy of original signals is the complex modulus of Fourier coefficients transformed from the signals. The actual domain of the frequency in (c) is from 0 to 1000 Hz.). This figure is available in colour online at wileyonlinelibrary.com/journal/espl

Data: Measuring and Filtering

Original impulsive signals and noise

Original data measured by the impact sensors are the voltage levels in millivolts. A millivolt change responds to about $760\,\mathrm{N\,m^{-2}}$ of impact pressure. The reference voltage level of each sensor was non-zero, and varied with the surges. The sampling frequency was set to $2\,\mathrm{kHz}$. The value of D_{50} of the three surges in

Figure 4 ranges from 7 to 10 mm. The frequency of particle impacts should be less than 1.8 kHz given that the mean diameter of grains is equal to D_{50} and that the maximum velocity is $12 \,\mathrm{m\,s^{-1}}$. Therefore, the sampling frequency is high enough to capture various impact pulses. The signals contained native random noise resulting from the measuring system and external disturbances, and real impact loading data were submerged in the background noise (Figure 6a). The mean value and standard deviation for the 50-second impulsive signal of the 12th surge are 80.4 and 19.4

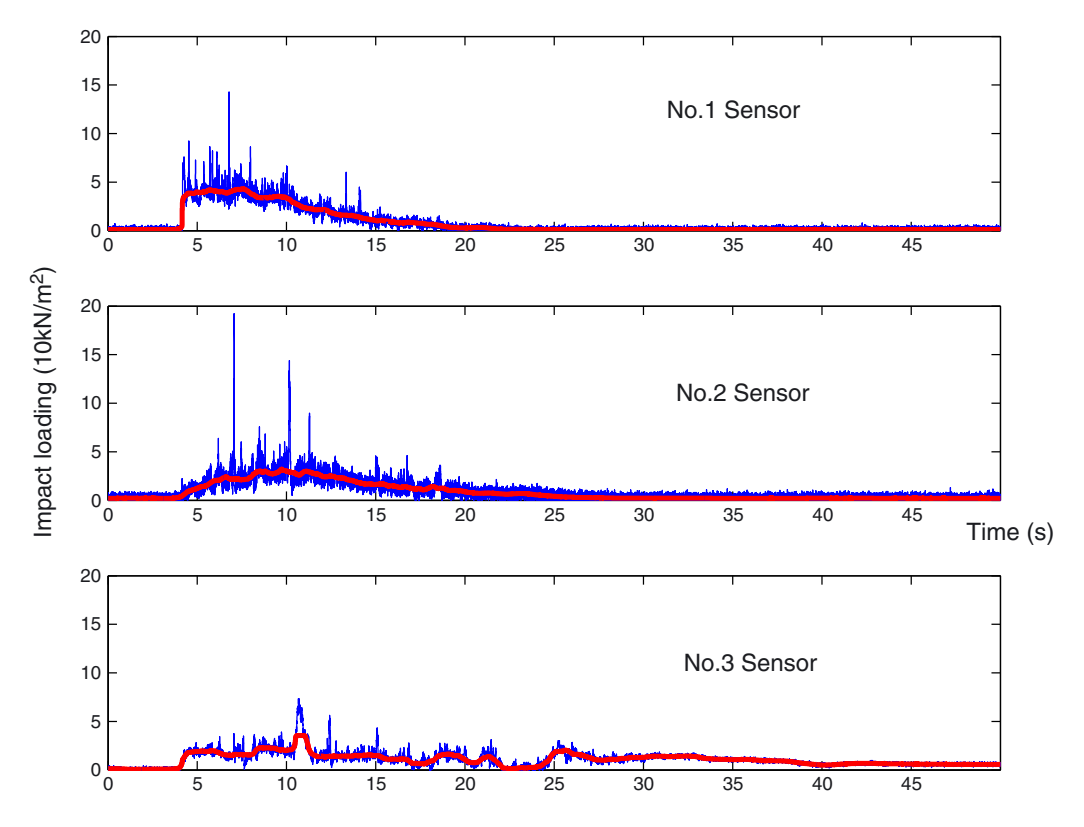


Figure 7. Time series of filtered impulsive loadings (in blue) and fluid pressure (in red) of the 12th surge. (The red data sequences resulting from the moving average with k = 2000 are considered as the long-term component of the blue data sequences, i.e. the fluid pressure.).

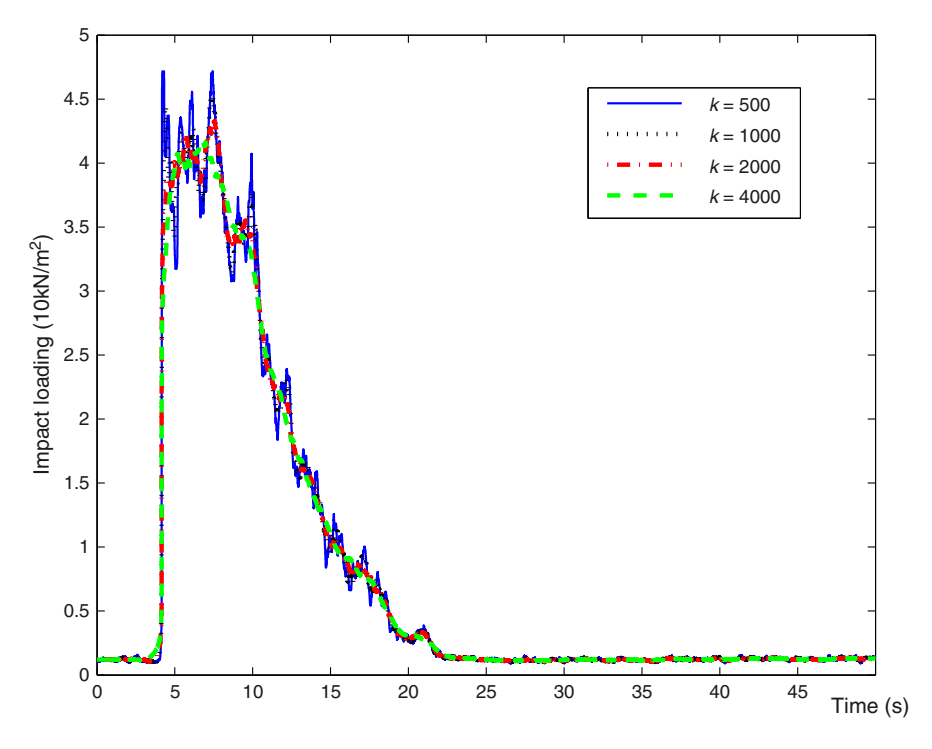


Figure 8. Separated components of the sensor 1 data of the 12th surge after averaged by four moving steps.

respectively. The histogram of the signals has two peaks (Figure 6b): one at 70 mV, corresponding to the reference voltage level without impact loading; and the other around 120 mV, corresponding to average hydrodynamic loading. Those signals of < 70 mV represented negative loadings caused by structure deflections. Sparse responses higher than 160 mV in the histogram indicated the existence of large boulder impacts. The dense part of the signals should be the high frequency component corresponding to background noise because the spectrum shows that the energy concentrates at low frequency (Figure 6c). Therefore, the high frequency component should be filtered from the original signals in order to recover the real pressure response.

Cut-off frequency of impulsive signals

The low pass filter is used to remove high frequency component and requires a cut-off frequency. Assuming that the particles in the surge fronts are spatially uniform along the flow direction and travel at the mean front velocity, we estimate the upper limit of the impact-loading frequency based on grain size distribution. The frequency f (in s^{-1}) is:

$$f = \frac{U}{I} \tag{1}$$

where U is the mean velocity of surge front (in m s⁻¹), I is the average interval between grains (in meters) and can be calculated by:

$$I = \left(\frac{1}{n}\right)^{1/3} \tag{2}$$

where n is the grain number per unit volume. If only the impacting of grains > 20 mm such as coarse gravels, cobbles or boulders is effective, the number n is

$$n = \sum_{i>20} \frac{V_i}{G_i} \tag{3}$$

where i indicates the grain size in millimeters, V_i is the total volume of grains with size i per unit volume (in m³), and G_i is the volume of an individual grain (in m³). All grains are regarded as spheres. Combining Equations 1–3 yields the impulsive frequency for the three samples. In practice, the grain size is divided into three intervals: [20, 40], [40, 80], and [80, 100]. Although it was observed that the particles larger than 100 mm existed in real flows (Figure 5), these particles can be ignored in Equation 3 because they are very rare in real flows. Then the upper frequencies of effective impacts for the three surges are 155·46, 179·95, and 188·66 Hz (Table III), respectively. Therefore, the cutoff frequency was set to 200 Hz, and the filtered impact loading data are shown in Figure 7.

Hydrodynamic and hydrostatic pressure

The filtered signals contain the slurry pressure and the grain impact loading. Three patterns of impacts have been identified: rectangular, saw-toothed, and peak-shaped (Zhang, 1993). The rectangular impulse results from a uniform fluid pressure while the peak impulse is from individual boulders. The impulse is generally saw-toothed due to boulders in the fluid. The long-term smooth component of the filtered signal is the sum of hydrostatic and hydrodynamic pressures caused by the slurry, while the

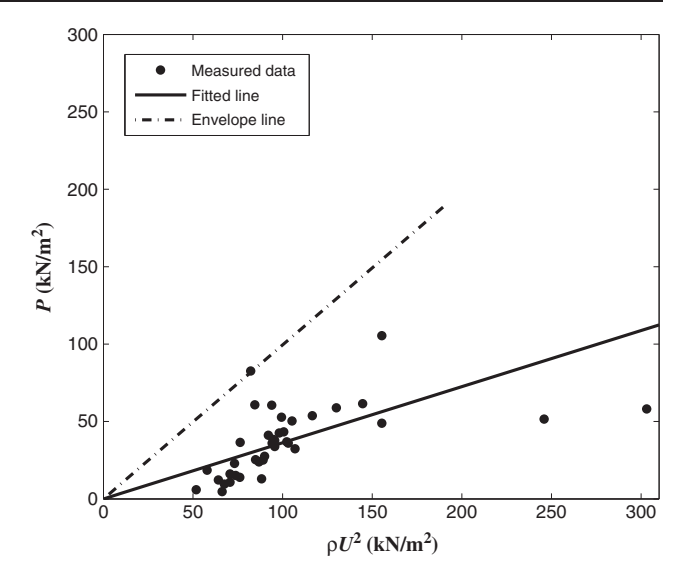


Figure 9. Maximum hydrodynamic pressure versus ρU^2 for 38 debrisflow surges.

random component is the impact loading caused by coarse grains. In order to eliminate the random component and keep the long-term response, we adopt the moving average method as in the following:

Nsg(i) =
$$\frac{1}{k} \sum_{j=0}^{k} sg(i+j)$$
 $i = 1, 2, ..., m-k; k < m$ (4)

where sg(i) is the value of ith point in the filtered data sequence, k is the step of moving average, Nsg(i) is the value of ith point in the new data sequence, and m is the total length of the filtered data sequence. We tested four steps of moving average with the impulsive loading data (Figure 8). The result of k= 2000 is less fluctuant than those of k= 500 and 1000, and has no big difference with k= 4000, which indicates the component separated by k= 2000 is suitable as the long-term response. The moving interval of 2000 is equivalent to a moving average time of one second, sufficiently long to eliminate the random component.

Results

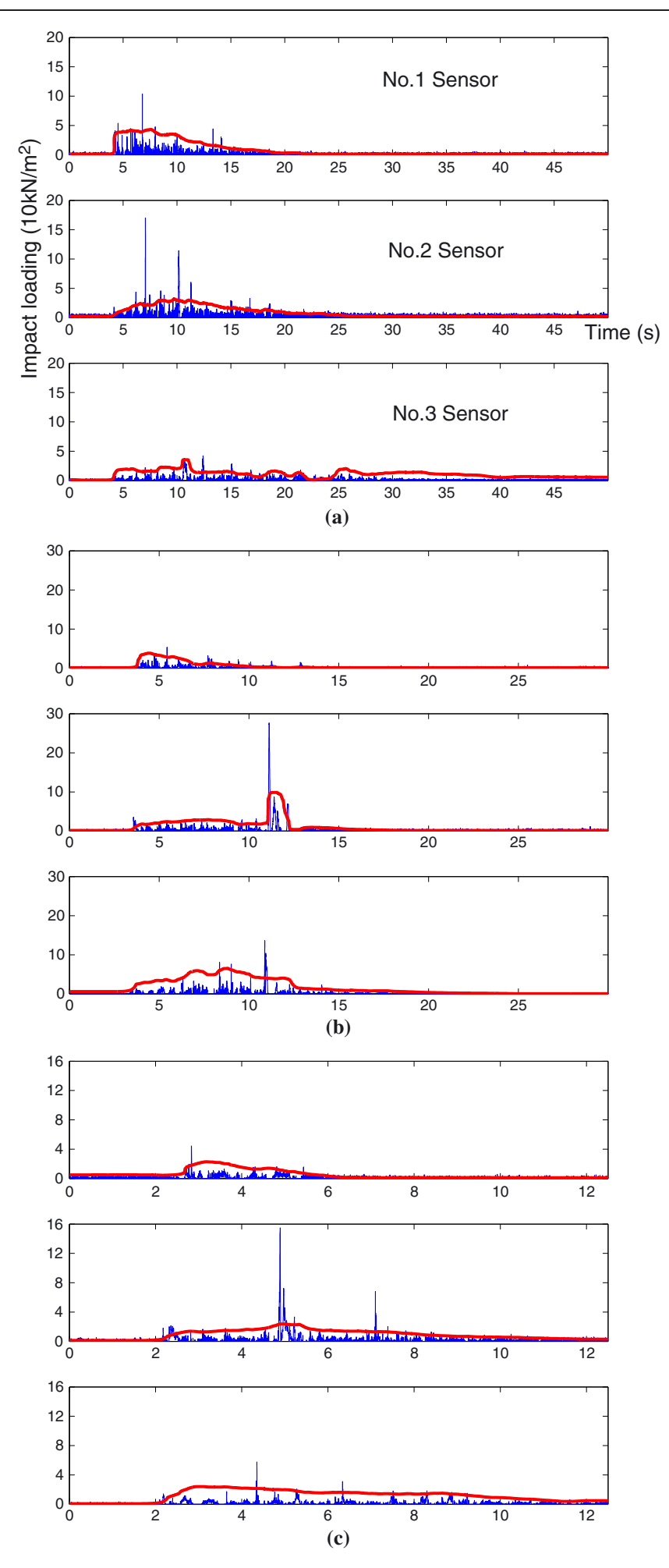
Mean velocity and hydrodynamic pressure

From the relationship, $F = c_d \rho Q U = c_d \rho S U^2$, the pressure is:

$$P = \frac{F}{S} = c_d \rho U^2 \tag{5}$$

where F is the impact force (in Newtons), $c_{\rm d}$ the empirical coefficient, Q the flow discharge passing through the column (in m³ s⁻¹), S the contact area (in m²), and P the complete impact pressure including the grain loading and fluid pressure (in N m⁻²). The value of $c_{\rm d}$ ranges widely because of the irregularity of the grain loading (Watanabe and Ikeya, 1981; Hungr et al., 1984; Armanini and Scotton, 1993; Zhang, 1993; Lo, 2000). In general, the relationship between the hydrodynamic pressure and ρU^2 is basic and simpler than that between P and ρU^2 . Study of the relationship is the first step for estimating $c_{\rm d}$. The coefficient is denoted by $c_{\rm hd}$ when P contains only the hydrodynamic pressure in Equation 5. Maximum hydrodynamic pressures and mean front velocities

Figure 10. Time series of the grain impact loading (in blue) and fluid pressure (in red) of the 12th (a), the 21st (b) and the 30th (c) surges. [Negative grain impact loading is not real and set to zero. The order of the sensors and the labels of *x*- and *y*-axes in (b) and (c) are the same as in (a).]



of 38 surges (Table IV) were used to find the empirical value of c_{hd} . Only the maximum hydrodynamic pressures measured by the first sensor were adopted because the hydrostatic pressure can be neglected for the first sensor so close to the flow <u>surface</u>. Least square fit of the data resulted in $c_{hd} = 0.362$ with a 95% confidence limit = [0·317, 0·408] but a poor correlation coefficient of 0.485 (Figure 9). The upper envelope line gives c_{hd} a maximum value of 1.01. This is smaller than the estimates by others (Table I) because what they estimated was actually the integrated coefficient c_d rather than c_{hd} . However, if we use the slurry bulk density of the 21st surge (1669 kg m⁻³), other than the debris-flow density (2180 kg m⁻³), c_{hd} will be equal to 0.473, approaching the coefficient of 0.5 for calculating the stagnation overpressure of incompressible fluid. Therefore, although the regression value of 0.362 is not good for c_{hd} , it reflects a rough trend between overpressure and velocity squared.

Grain impact loading

Subtracting the fluid pressure from the total impulsive loading in Figure 7, the series grain impact loading was obtained and compared with that of the fluid pressure (Figure 10). The sharp grain impact loading is random and does not increase with fluid pressure. The responses of impact force at three depths are not synchronous. The first sensor recorded more grain impacts at the surge front while the third recorded notable grain impacts even at the tail 20 seconds later, revealing the vertical distinction of grain distribution in the surge. Large grains are prone to concentrate in the surface and middle parts of the flow. This is indirect evidence for a vertical reverse segregation of size in debris flows (equivalent to inverse grading in a deposit).

The ratios of the maximum grain impact loading to the fluid pressure are different at the three depths for the 12th surge: $2\cdot39$ for the first, $5\cdot29$ for the second, and $1\cdot19$ for the third (Figure 10a). Both experimental studies and field observations indicate that impact forces by coarse grains are much larger than the fluid pressure (Hungr *et al.*, 1984; Zhang 1993; Haehnel and Daly, 2004). It is readily seen from Table IV that the highest ratio of grain impact loading to fluid pressure is $44\cdot34$ for the 35th surge, and the value of $c_{\rm d}$ ranges from $0\cdot30$ to $11\cdot1$. The grain loadings at the first sensor exceed $1000\,{\rm kN}~{\rm m}^{-2}$ for 8th and 19th surges, corresponding to two extreme values of the coefficient. It is noted that the flow depth has a strong influence on grain impact as well as on mean velocity.

Discussion

The above analysis does not take into account the influences of structure deformation or of the impact sensor's size. Actually, the existence of voltage levels less than the no-loading level in Figure 6b indicates the influence of deformation. The minimum, no-loading and maximum voltage values are 43, 70 and 269 mV during the 12th surge. Given that the minimum value can be completely ascribed to structure deformation, the possible negative loading was up to 13.6% of the peak impact loading. Therefore, the structure deformation could reduce the impact force and hence the value of c_d to some extent. Unfortunately, we have no further evidence to enable an accurate estimation of the deformation effect. The situation is more difficult with respect to the size of the sensors. Our data measured by sensors of the same size do not allow us to make a quantitative analysis of this kind of influence. Intuitively, a large sensor has a higher probability of being impacted by

particles, and particle impacts on a small sensor will probably be more erratic. This means that the signals measured by a large sensor are smoother than those measured by a small one, and will yield fewer abnormal values.

The hydrostatic and hyrdodynamic models are the most popular among the hydraulic models because debris-flow velocity and front height are more easily acquired than variables such as shock wave speed, applied in other models. The key issue is determination of the coefficient. For a hydrodynamic model, the values of the coefficient based on laboratory tests are 0·2-2·2 (Armanini and Scotton, 1993), and 1·25-3·75 (Scotton and Deganutti, 1997), and are between 0.38 and 18.67 based on the field data of eight torrents (Hübl et al., 2009). Zhang and Yuan (1985) reported a range from 1.4 to 8.1 over 24 debris-flow surges at Jiangjia Ravine in 1975. These studies may slightly overestimate the coefficient, for lack of extracting the long-term component from complete impact pressure data. However, differences with other studies can be attributed primarily to different types of debris flows such as flow regime, or to different proportions of granular components. Lo (2000) suggested that the debris impact pressure could be taken as at least three times the value of ρU^2 . Other researchers recommended the value of c_d as between 2.0 and 5.0 (Watanabe and Ikeya, 1981; Zhang, 1993). The coefficient c_d of our field data exceeds 3·0 in only four out of 38 surges (5th, 8th, 16th, and 19th). The outlier values are due to extreme collisions caused by large boulders, and depend on the maximum size of boulders that debris flows can carry. Although Hungr et al. (1984) suggested that the maximum diameter of boulders in design could be assumed equal to the flow depth, it is still difficult to get the impact effect because the collision is influenced by many unpredictable factors such as impact orientation, contact area, run-up height, and the grain size and its distribution. Therefore, the maximum value of c_d measured in this test is not the upper limitation. Application of these results to the design of mitigation measures should be cautious, especially when very large boulders may be transported.

For a hydrostatic model Armanini and Scotton (1993) and Scotton and Deganutti (1997) presented the coefficient $c_{\rm s}$ as between 2·5–7·5 based on laboratory experiments (Table I). Applying the hydrostatic formula to the Jiangjia data of 2004, $c_{\rm s}$ exhibits a wide range from 1·89 to 44·57, and there are seven surges in which $c_{\rm s}$ is larger than 7·5. It appears that the hydrodynamic model is better than the hydrostatic as describing the impact force of debris flows in the field. Furthermore, extending our analysis to a mixed model like that of Arattano and Franzi (2003) (Table I), the coefficient $c_{\rm m}$ from the Jiangjia data is between 0·28 and 9·88, and is larger than 3·0 only for three surges. The better result for $c_{\rm m}$ suggests that the mixed model with $c_{\rm m}$ = 3·0 is acceptable for estimating the impact force in most cases.

Conclusions

Debris-flow impact is difficult to measure directly in the field. A new test system set up at Jiangjia Ravine successfully measured the impact processes of moderate-scale debris flows occurring on August 25, 2004. This is the first time a long-duration series of impact force was measured at different flow depths. Coarse grains play a key role in the impact force. The upper limit of grain-impact frequency is calculated at 188·66 Hz from the grain size distribution of three debris-flow samples. Therefore, background noise can be removed from the original signals by a low-pass filter with a cut-off frequency of 200 Hz. The fluid pressure and the grain-impact loading, which are considered

as the long-term and random component of the filtered impulsive signals and decomposed by the moving average method, do not exhibit similar behaviors. The impact loadings are far greater than the fluid pressures and are non-synchronous at the three flow depths. Based on the experimental data, it is found that the coefficient $c_{\rm hd}$ of the hydrodynamic pressure is equal to 0.362 while the coefficient $c_{\rm d}$ of the complete impact pressure can reach to 11.1, which is helpful for guiding the design of engineering structures designed to mitigate debris-flow damage.

Acknowledgments—This work was financially supported by National Natural Science Foundation of China (Grant No. 40771026 and 40701014) and Project Group of Knowledge Innovation Program of Chinese Academy Sciences (KZCX2-YW-Q03-5). The authors thank the Dongchuan Debris Flow Observation and Research Station, Chinese Academy of Sciences for providing the experimental facilities. The authors are also grateful to Professor Vincenzo D'Agostino, Dr Brian McArdell and another anonymous reviewer for their beneficial comments. Special thanks are due to Professor Kevin M. Scott for his careful revision.

References

- Arattano M. 2000. On debris flow front evolution along a torrent. *Physics and Chemistry of the Earth (B)* **25**(9): 733–740.
- Arattano M, Franzi L. 2003. On the evaluation of debris flows dynamics by means of mathematical models. *Natural Hazards and Earth System Sciences* **3**: 539–544.
- Armanini A. 1997. On the dynamic impact of debris flows. In *Recent Developments on Debris Flows*, Armanini A, Michiue AM (eds). Springer-Verlag: Berlin; 208–225.
- Armanini A, Scotton P. 1993. On the dynamic impact of a debris flow on structures, *Proceedings of XXV Congress of IAHR*, Tokyo; 203–210.
- Cui P, Chen X, Wang Y, Hu KH, Li Y. 2005. Jiangjia Ravine debris flows in south-western China. In *Debris-flow Hazards and Related Phenomena*, Jakob M, Hungr O (eds). Springer-Praxis: Berlin; 565–594.
- D'Agostino V, Casonato A. 2000. Dynamic impact hypotheses for designing check dams involved in debris flow phenomena. In *Proceedings of the International Workshop "Los alludes torrencial de Diciembre 1999 en Venezuela"*. Caracas: Facultad de Ingegneria, Instituto de Mecanica de Fluidos.
- Haehnel RB, Daly SF. 2004. Maximum impact force of woody debris on floodplain structures. *Journal of Hydraulic Engineering ASCE* **130**(2): 112–120.
- Hu KH, Wei FQ, Hong Y, Li XY. 2006. Field measurement of impact force of debris flow. *Chinese Journal of Rock Mechanics and Engineering* **25**(Supp. 1): 2813–2819 (in Chinese).
- Hübl J, Holzinger G. 2003. Entwicklung von Grundlagen zur Dimensionierung kronenoffener Bauwerke für die Geschiebebewirtschaftung in Wildbächen: Kleinmaßstäbliche Modellversuche zur Wirkung von Murbrechern. WLS Report 50 Band 3. Im Auftrag des BMLFUW VC 7a
- Hübl J, Suda J, Proske D, Kaitna R, Scheidl C. 2009. Debris flow impact estimation. *Proceedings of the International Symposium on Water Management and Hydraulic Engineering*, 1–5 September, Ohtid, Macedonia.
- Hungr O, Morgan GC, Kellerhals R. 1984. Quantitative analysis of debris torrent hazard for design of remedial measures. *Canadian Geotechnical Journal* 21: 663–677.
- Iverson RM. 1997. Physics of debris flows. *Reviews of Geophysics* **35** (3): 245–296.
- Li J, Yuan JM. 1983. The main features of the mudflow in Jiang-Jia Ravine. *Zeitschrift fuer Geomorphologie N.F.* **27**(3): 325–341.
- Lin PS, Chang WJ, Liu KS. 1997. Retaining function of open-type sabo dams. In *Debris Flow Hazards Mitigation: Mechanics, Prediction,* and Assessment. ASCE: New York; 636–645.

- Liu KF, Lee FC, Tsai HP. 1997. The flow field and impact force on a debris dam. In *Debris Flow Hazards Mitigation: Mechanics, Prediction, and Assessment*. ASCE: New York; 737–746.
- Lo DOK. 2000. Review of Natural Terrain Landslide Debris-resting Barrier Design, Geotechnical Engineering Office, Geo Report No. 104. Civil Engineering Department: Government of the Hong Kong Special Administrative Region.
- Marchi L, Arattano M, Deganutti AM. 2002. Ten years of debris-flow monitoring in the Moscardo Torrent (Italian Alps). *Geomorphology* **46**: 1–17
- Mizuyama T. 1979, Computational method and some considerations on impulsive force of debris flow acting on sabo dams. *Journal of the Japan Society of Erosion Control Engineering* **112**: 40–43 (in Japanese).
- Okuda S, Suwa H, Okunishi K, Nakano M, Yokoyama K. 1977. Synthetic observation on debris flow, Part 3. Observation at Valley Kamikamihorizawa of Mt Yakedake in 1976. *Annuals of Disaster Prevention Research Institute, Kyoto University* **20B-1**: 237–263 (in Japanese).
- Revellino P, Hungr O, Guadagno FM, Evans SG. 2004. Velocity and runout simulation of destructive debris flows and debris avalanches in pyroclastic deposits, Campania region, Italy. *Environmental Geology* 45(3): 295–311.
- Scotton P, Deganutti AM. 1997. Phreatic line and dynamic impact in laboratory debris flow experiments. In *Debris Flow Hazards Mitigation: Mechanics, Prediction, and Assessment*. ASCE: New York; 777–786.
- Shieh CL, Ting CH, Pan HW. 2008. Impulsive force of debris flow on a curved dam. *International Journal of Sediment Research* **23**(2): 149–158.
- Suwa H, Okuda S, Yokohama K. 1973. Observation system on rocky mudflow. *Bulletin of the Disaster Prevention Research Institute, Kyoto University* **23**: 59–73.
- Watanabe M, Ikeya H. 1981. Investigation and Analysis of Volcanic Mud Flows on Mount Sakurajima, Japan. Erosion Sediment Transport Measurement. International Association on Hydrology: Florence; Science Publication 133/1981, 245–256.
- Wei F, Zhang Y, Hu KH. 2006. Model and method of debris flows risk zoning based on momentum analysis. *Wuhan University Journal of Natural Sciences* **11**(4): 835–839.
- Wei H. 1996. Experimental study on impact force of debris flow heads. *Chinese Railway Science* **17**(3): 50–61 (in Chinese).
- Wendeler C, Volkwein A, Roth A, Denk M, Wartmann S. 2007. Field measurements used for numerical modelling of flexible debris flow barriers. In *Debris-Flow Hazards Mitigation. Mechanics, Prediction,* and Assessment, Chen C-I, Major JJ (eds). Millpress:Rotterdam; 681–687.
- Wu J, Kang Z, Tian L, Zhang S. 1990. *Observation and Research of Debris Flows at Jiangjia Basin in Yunnan Province*. Science Press: Beijing (in Chinese).
- Zanchetta G, Sulpizio R, Pareschi MT, Leoni FM, Santacroce R. 2004. Characteristics of May 5–6, 1998 volcaniclastic debris flows in the Sarno area (Campania, southern Italy): relationships to structural damage and hazard zonation. *Journal of Volcanology and Geothermal Research* 133(1–4): 377–393.
- Zanuttigh B, Lamberti A. 2006. Experimental analysis of the impact of dry avalanches on structures and implication for debris flows. *International Journal of Hydraulic Resources* **44**(4): 522–534.
- Zhang S. 1993. A comprehensive approach to the observation and prevention of debris flows in China. *Natural Hazards* 7: 1–23.
- Zhang S, Yuan J. 1985. Impact force of debris flow and its detection. In *Memoirs of Lanzhou Institute of Glaciology and Cryopedology of Chinese Academy of Sciences (No. 4)*. Science Press: Beijing; 269–274 (in Chinese).
- Zhang Y, Wei FQ, Wang Q. 2007. Experimental research of reinforced concrete buildings struck by debris flow in mountain areas of western China. *Wuhan University Journal of Natural Sciences* **12**(4): 645–650.